Potential-Induced Defects in *n*-Alkanethiol Self-Assembled Monolayers Monitored by Impedance Spectroscopy

Emmanuelle Boubour and R. Bruce Lennox*

Department of Chemistry, McGill University, 801 Sherbrooke West, Montréal Québec, Canada H3A 2K6

Received: January 11, 2000; In Final Form: June 28, 2000

The ionic permeability of alkanethiol self-assembled monolayers (SAMs) chemisorbed on gold is studied using ac impedance spectroscopy in the absence of redox active species. $CH_3(CH_2)_nS/Au$ ($n = 7-15$) SAMs behave as ionic insulators until a critical potential, V_c, is reached or exceeded. At potentials more cathodic than V_c, SAMs are no longer ionic insulators and a significant change in the phase angle is associated with ion penetration in the low-frequency region. V_c is chain length dependent and is observed at potentials (−0.15 to −0.35 V vs Ag/AgCl) that are considerably more anodic than the alkanethiol electrodesorption potential. The relaxation frequency of trans-SAM ion migration (4−100 Hz) can be calculated from fitting of the impedance data to an appropriate equivalent circuit or from Bode phase plots.

Introduction

Self-assembled monolayers (SAMs) are of great interest since they allow one to deliberately derivatize metal (Au, Pt, Cu, Ag, Hg) and semiconductor (Si, Ge, GaAs, CdSe, CdS, InP, $MoSe_2$, and MoS_2) substrates with a chemically well-defined organic ultrathin film, in a relatively facile and reliable manner. The applications of SAMs include work function modulation of metals and semiconductors,[1−7] nano-FETs,[8,9] and biosensor construction.[10−13] SAMs are also ideal components in impedimetric sensors, given that they may be used to directly detect a specific binding event.[14]

n-Alkanethiol ($CH_3(CH_2)_nS/Au$) SAMs have been particularly well studied using a number of bulk and surface sensitive techniques. These include contact angle, ellipsometry, Fourier transform infrared (FT-IR) and Raman spectroscopies, surface plasmon resonance, He diffraction, X-ray photoelectron spectroscopy (XPS), second harmonic generation spectroscopy (SHG), X-ray diffraction, ultrahigh vacuum scanning tunneling microscopy (UHV-STM), atomic force microscopy (AFM), temperature-programmed desorption (TPD) , and electrochemistry.[15] Issues such as the presence and size of pinhole defects,[16−19] phase transitions,[20] and domain formation have been of particular interest as they relate to the quality of the film.

Only a limited number of studies have considered $CH_3(CH_2)_nS/Au$ SAMs as models of supported lipid membranes (s-BLMs), despite the obvious structural parallels. The permeability properties of s-BLMs and black lipid membranes (BLMs) under applied electric fields are of importance because they themselves are excellent models of cell membranes. These artificial phospholipid membrane-based systems provide detailed information about membrane conductance as a function of the applied electric field, as well as details about ion and water translocation in the membrane. While most s-BLM and BLM studies use dc electrochemical techniques, ac impedance spectroscopy has provided a better understanding of how transmembrane ion transport is modulated by ion carriers or peptide channels.[13,21−33]

A tentative link between lipid membranes and $CH_3(CH_2)_nS/Au$ SAMs was revealed in our earlier work, where $CH_3(CH_2)_nS/Au$ SAMs exhibit the same phase transition temperatures as the phospholipid membranes of equivalent chain length. With $Fe(CN)_6^{3-/4-}$ as a permeability probe, it was shown that SAMs can mimic phospholipid membranes in regard to their permeability features.[20] The effect of applied potential on SAMs has not received detailed attention however. The perturbation of BLMs by large electric fields is well-established[34,35]and indeed is the basis of the electroporation technique used in cell biology. A very recent study by Haag et al. probing the factors that control the dielectric breakdown of SAMs in a Hg/SAM-SAM/metal (Au, Ag, Hg) configuration suggests that parallels between BLMs and SAMs may indeed exist.[36]

In this study, we have undertaken to define the relationship between the alkyl chain length of SAMs and their permeability properties using ac impedance spectroscopy in the absence of an electrochemical redox couple. We probe how an applied dc voltage (between +0.4 and −0.5 V vs Ag/AgCl) modulates alkanethiol SAM structure. Reductive electrodesorption of alkanethiol chains is observed at much more reductive potentials (∼−1 to −1.4 V vs Ag/AgCl for $n = 7-15$) than the working potential window used in this study.[37−43] We also explore parallels between $CH_3(CH_2)_nS/Au$ systems and BLM and s-BLM systems.[12,22,24−26,31,44,45] The broad time scale spanned by ac impedance spectroscopy (microseconds to seconds) makes it possible to relate changes in the dielectric properties of SAMs to molecular mechanisms. The effect of a transmembrane electrical potential on *n*-alkanethiol SAMs of various chain lengths ($n = 7-15$) will be discussed in terms of electrochemical stability, permeability to electrolyte ions, and variation in the SAM microstructure.

Experimental Section

Instrumentation. Electrochemical impedance spectroscopy (EIS) measurements were obtained in a conventional three-electrode electrochemical cell with an EG&G lock-in amplifier (5210) combined to an EG&G PAR 273 potentiostat/galvanostat. The counter electrode was a platinum mesh (Aldrich, Milwaukke, WI) and the reference electrode was a Ag/AgCl

* To whom correspondence should be addressed. Fax: 514-398-3797. Tel: 514-398-3638. E-mail: Bruce_Lennox@maclan.mcgill.ca.

10.1021/jp000151o CCC: $19.00
Published on Web 09/02/2000

electrode (3 M NaCl, Bioanalytical Systems Inc., West Lafayette, IN). Data acquisition was performed using EG&G M398 software. A sinusoidal potential modulation of ±10 mV amplitude was superimposed on a fixed dc potential. The amplitude and the phase shift of the resulting current were recorded at each frequency (15 points per decade equally spaced on a log scale).

The effect of the applied potential on SAM permeability was investigated from +0.4 to −0.5 V in 0.1 V steps. The time duration of each experiment was 30 min. The impedance data were then transferred to the Z plot/Z view software package (Scribner Associates Inc., Southern Pines, NC) and were fitted to an electrical equivalent circuit using the Complex Nonlinear Least Square (CNLS) Immittance Fitting Program.[46] The equivalent circuit provides an electrical analogue of chemical/physical processes probed by ac EIS.[47] On each impedance graph, symbols represent the raw experimental data and the solid lines result from CNLS data fits. The solution resistance, R_s, is 300 ± 25 Ω (for an electrolyte of 50 mM K_2HPO_4, pH 7.0). A Teflon cover was used to close the electrochemical cell and to position the three electrodes in a reproducible manner, minimizing experiment-to-experiment variation.

Chemicals. Octanethiol (98.5%), decanethiol (97%), and dodecanethiol (98%) were purchased from Aldrich (Milwaukee, WI) and were used as received. Hexadecanethiol was available from previous studies and was synthesized from 1-bromohexadecane (97% Aldrich) by standard procedures.[48]

$HS(CH_2)_{15}CH_3$: mp 19.5−21 °C; TLC (silica gel, *n*-hexane) $R_f = 0.7$; ^{1}H NMR (500 MHz, $CDCl_3$, 25 °C) δ 2.52 (q, 2H, C*H*$_2$SH), 1.58 (m, 2H C*H*$_2$CH$_2$SH), 1.40 (m, 2H, C*H*$_2$CH$_2$CH$_2$-SH), 1.31 (t, 1H, CH$_2$S*H*), 1.24 (s, 24H, (C*H*$_2$)$_{12}$), 0.87 (t, 3H, C*H*$_3$).

Dibasic potassium phosphate was ACS reagent grade (BDH, Montreal, Canada).

Procedure. Polycrystalline gold electrodes (0.020 cm^2 geometric surface area) were purchased from Bioanalytical Systems Inc. (West Lafayette, IN) and were mechanically hand polished on microcloth pads (Buehler) with alumina slurries (Buehler) of decreasing particle size (1.0, 0.3, and 0.05 μm). The polished electrodes were sonicated in ultrapure water (Milli-Q water system, 18 MΩ cm) in an ultrasonic bath (Branson 1200) for 2 min. The electrodes were then immediately cleaned with freshly prepared aqua regia solution (60% v/v water, 30% hydrochloric acid and 10% nitric acid). This step was immediately followed by the electrochemical polishing of the gold surface between 0 and +1.7 V (vs Ag/AgCl) at 80 mV s^{-1} in N_2-purged 1 M perchloric acid (HPLC grade, BDH). The electrodes were then thoroughly rinsed with ultrapure water and absolute ethanol (Commercial Alcohols Inc., Brampton, Canada) prior to incubation in a N_2-purged 1 mM $CH_3(CH_2)_nSH$ solution, at room temperature, in sealed vials. The electrodes were incubated for a minimum of 72 h. Prior to each measurement, the SAM-coated electrodes were rinsed with a copious amount of absolute ethanol followed by ultrapure water. Impedance spectra were obtained at room temperature after a stable open circuit potential was reached.

Data Analysis. Special care must be taken when analyzing impedance spectra, particularly with biological tissues, living cells, and membrane models such as SAMs.[49] Data interpretation from impedance spectra can depend on the way the data are represented, where two main types of representations are often used. An Argand diagram plots the imaginary component of a parameter (impedance *Z*, capacitance *C*, or the dielectric constant ϵ) vs its real component. A Bode diagram plots the modulus of a given parameter ($|Z|$ or $|C|$ or the phase angle φ) as a function of the frequency, *f*. The graphical interpretation of the raw data can further influence modeling of the experimental results. For example, ion-diffusion processes occur in the low frequency domain ($\leq\sim10^2$ Hz) and they are thus more apparent in Bode plots (φ vs *f*) than in Argand diagrams (Z'' vs Z') or in $|Z|$ vs *f*. A comparison of these three representations also assists in judging the validity of data fitting over the entire experimental frequency domain probed.

Results and Discussion

$CH_3(CH_2)_nS$/Au SAMs reported in this study were first analyzed by ac EIS at a benign dc potential (i.e., nonaltering to the SAM)[50] in 50 mM K_2HPO_4 at pH 7.0. $CH_3(CH_2)_nS$/Au SAMs behave as capacitors at +0.4 V (vs Ag/AgCl), exhibiting a phase angle $\varphi \geq 88°$ at 1 Hz $< f <$ 10^3 Hz (cross symbols in Figure 1a). From an electrical circuit perspective, a pure capacitor (in absence of leakage current) has a phase angle $\varphi = 90°$ over the entire frequency domain. On the other hand, $\varphi = 0°$ for a pure resistor.[47] SAMs are practically defect-free when $\varphi \geq 88°$ in the medium-to-low-frequency region ($1 \leq f \leq \sim10^3$ Hz).[50] A frequency of 1 Hz is used as the lowest observation frequency in this study because, when $f < 1$ Hz, the data acquisition can take minutes and the electrochemical response may no longer be linear.

1. Effect of dc Potential on the Phase Angle and SAM Capacitance. The effect of an applied dc potential, V_{appl}, at either −0.4 or −0.5 V (vs Ag/AgCl) on a $CH_3(CH_2)_{15}S$/Au SAM is shown in Figure 1. Raw data (symbols) and CNLS simulations (solid lines) are displayed using three different impedance representations (Figures 1a-c). When $V_{appl} > -0.4$ V (i.e., from −0.3 to +0.4 V), the phase angle remains ≥88° (cross symbols), even in the lowest frequency domain probed (1 Hz $\leq f \leq$ 50 Hz). Therefore, at −0.3 V $\leq V_{appl} \leq$ +0.4 V, the data can be fitted to the Helmholtz parallel plate capacitor model,[51,52] whose equivalent circuit involves a solution resistance in series with a constant phase element, CPE (equivalent circuit I in Figure 2).[50] The CPE corresponds to the SAM capacitance and its exponent *n* is ∼0.98.

At −0.4 V for $n = 15$ and beyond, φ in the low frequency domain deviates from 88° (Figure 1a). This decrease in φ occurs when $V_{appl} \leq -0.3$ V for $n = 11$ (Figure 3a) and $V_{appl} \leq -0.2$ V for $n = 7$ (Figure 4a) and is more accentuated as the applied potential becomes increasingly cathodic. These results demonstrate that for each chain length *n*, the SAM no longer behaves as a capacitor once a particular potential is exceeded. We refer to this experimental potential as the critical potential (V_c). An equivalent circuit different from I is necessary if one is to obtain an adequate fit to the data at $V_{appl} \leq V_c$ (II in Figure 2). The fit to equivalent circuit II at $V_{appl} \leq V_c$ is excellent in all frequency regions, except for small deviations in the 5−30 Hz range. Attempts to improve the fit by introducing a CPE instead of C_m does not provide a better fit. The physical interpretation of each of the components (C_m, R_m, C_d, and R_d) is presented later in the discussion.

The electrochemical signal change associated with $V_{appl} \leq V_c$ in the low frequency domain for $n = 7-15$ is also observed in Bode plots, $|Z|$ vs *f* (Figures 1b, 3b, and 4b), but not as prominently as in the Bode phase plots, φ vs *f* (Figures 1a, 3a, and 4a). The corresponding Nyquist plots Z'' vs Z' (Figures 1c, 3c, and 4c) also demonstrate that V_{appl} affects the interfacial properties of SAMs. For example, at −0.5 V ($n = 15$), the data deviate significantly from the vertical line observed at $V_{appl} >$ −0.3 V (cross symbols).

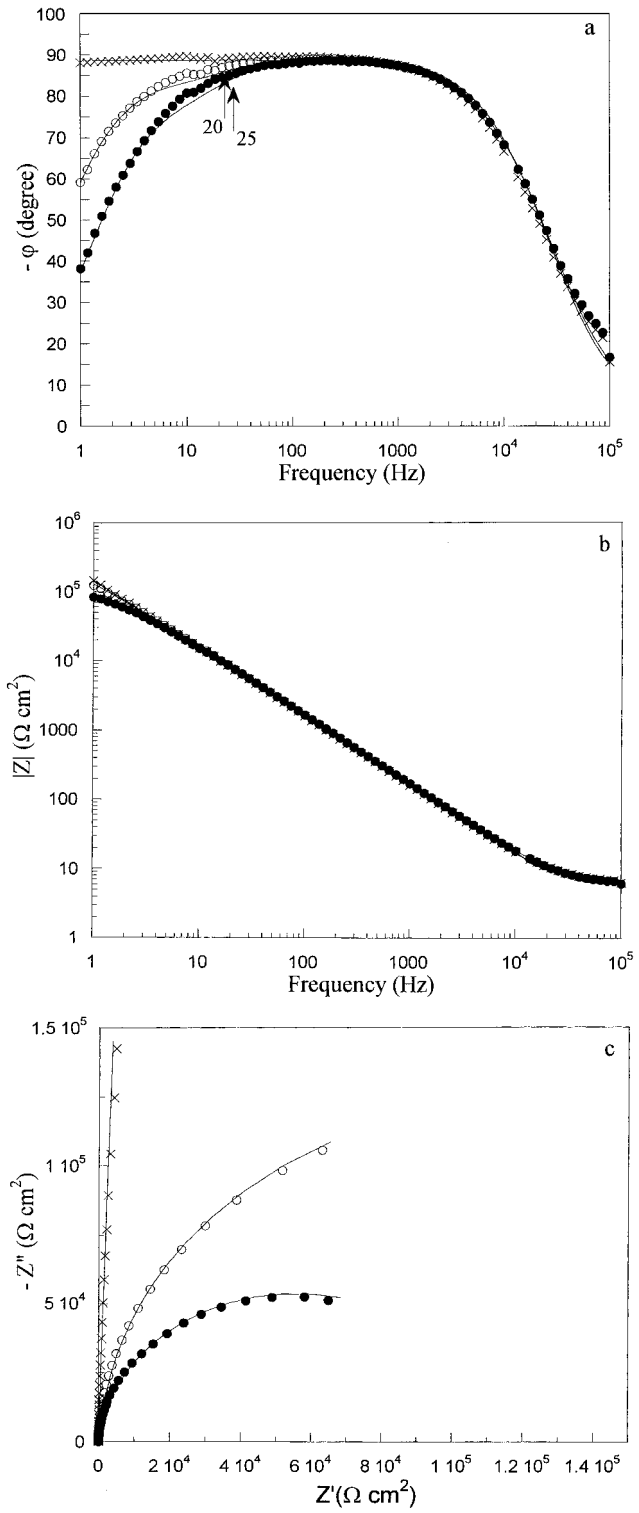

Figure 1. (a) Bode phase plot, (b) Bode plot, and (c) Nyquist plot of a $CH_3(CH_2)_{15}S$/Au SAM from +0.4 V (vs Ag/AgCl) to −0. 3 V (×) (equivalent circuit I), at −0.4 V (○) and −0.5 V (●) (equivalent circuit II) in 50 mM K_2HPO_4, pH 7.0. Symbols are the experimental data points, and solid lines result from CNLS data fits, according to the equivalent circuits. The numbers in (a) correspond to the relaxation frequency, ν_d, tabulated in Table 1.

The critical potential V_c is determined from the interpolation of the phase angle at 1 Hz (φ_{1Hz}) vs V_{appl} and corresponds to the potential where φ_{1Hz} deviates significantly from 88°. V_c depends on the alkyl chain length and ranges from −0.35 V vs Ag/AgCl ($n = 15$) to −0.25 V ($n = 11$) to −0.15 V ($n = 7$). We believe the changes in the electrochemical responses at

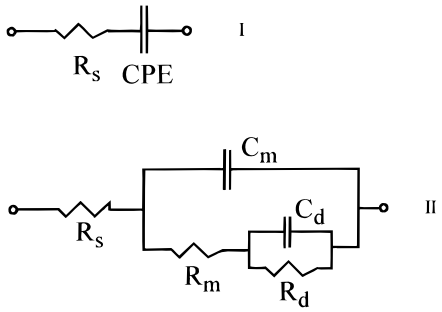

Figure 2. Equivalent circuit (I) of a defect-free $CH_3(CH_2)_nS$/Au SAM (i.e., at $V_{appl} > V_c$) and (II) of a SAM presenting potential-induced defects at $V_{appl} \leq V_c$ (II). R_s is the solution resistance (350 ± 25 Ω). The CPE (constant phase element) and C_m represent the SAM capacitance. In (II), R_m is the SAM resistance. C_d and R_d account for the deliberately formed defects induced at $V_{appl} \leq V_c$.

$V_{appl} \leq V_c$ are associated with molecular changes within the SAM, at the SAM/electrolyte interface, or both. The range of potentials over which the SAMs undergo changes depends on the SAM chainlength, and V_c corresponds to the onset of film perturbation.

A recent AFM/electrochemical study showed that a CH_3-CH_2S/Au SAM undergoes a transformation at −0.12 V (vs SCE). This is unrelated to the reductive desorption process that occurs at −0.31 V for this chain length.[53] This film transformation involves the formation of small islands and is reversible when the electrode is polarized to more positive potentials, typically +0.2 V. We believe that longer alkyl chain SAMs studied here are subjected to a similar process. V_c is apparently linked to a film transformation and can effectively be probed by ac EIS. We show below that this film transformation is strongly associated with the formation of potential-induced defects in *n*-alkanethiol SAMs and that these disruptions are not completely reversible.

Equivalent circuit II is used for $CH_3(CH_2)_nS$/Au SAMs ($n = 7-15$) when $V_{appl} \leq V_c$ and yields a good fit (solid lines) to the experimental data (symbols) (Figures 1, 3, and 4). This equivalent circuit is also appropriate in describing corrosion processes in polymer-coated metals,[54] water uptake during polymer degradation,[55] oxygen diffusion into *n*-alkanethiol SAMs adsorbed onto copper,[56] and Cs^+ selective transport in s-BLMs doped with Gramicidin D.[22] The CNLS fit also provides the value of each component (C_m, R_m, C_d, and R_d) for equivalent circuit II (Table 1). The SAM capacitance (C_m) is not affected by the applied potential over the range of +0.4 V to −0.5 V (vs Ag/AgCl), as per cyclic voltammetry studies.[57-62] The other parameters (R_m, C_d, and R_d) do, however, vary with V_{appl}.

The SAM resistance, R_m, reflects the ion/water migration within the SAM. R_m is affected by the formation or enhancement of defects and gradually decreases as V_{appl} becomes increasingly cathodic. R_d describes the ease of moving an ion from the interface to the SAM,[31,33] given that R_d in lipid membrane studies is a phase transfer resistance associated with the transport of ions from the solution into the membrane. As the applied electric field increases in magnitude, the energy required for ion transfer into the SAM decreases, leading to a substantial decrease in R_d. The capacitance of defects, C_d, reflects the ability of the SAM to store ions. C_d increases when V_{appl} is polarized at increasingly cathodic potentials.

The nature of the dependence of R_m, R_d, and C_d on V_{appl} indicates that the electric field induces changes at the SAM/electrolyte interface and facilitates the permeation of water

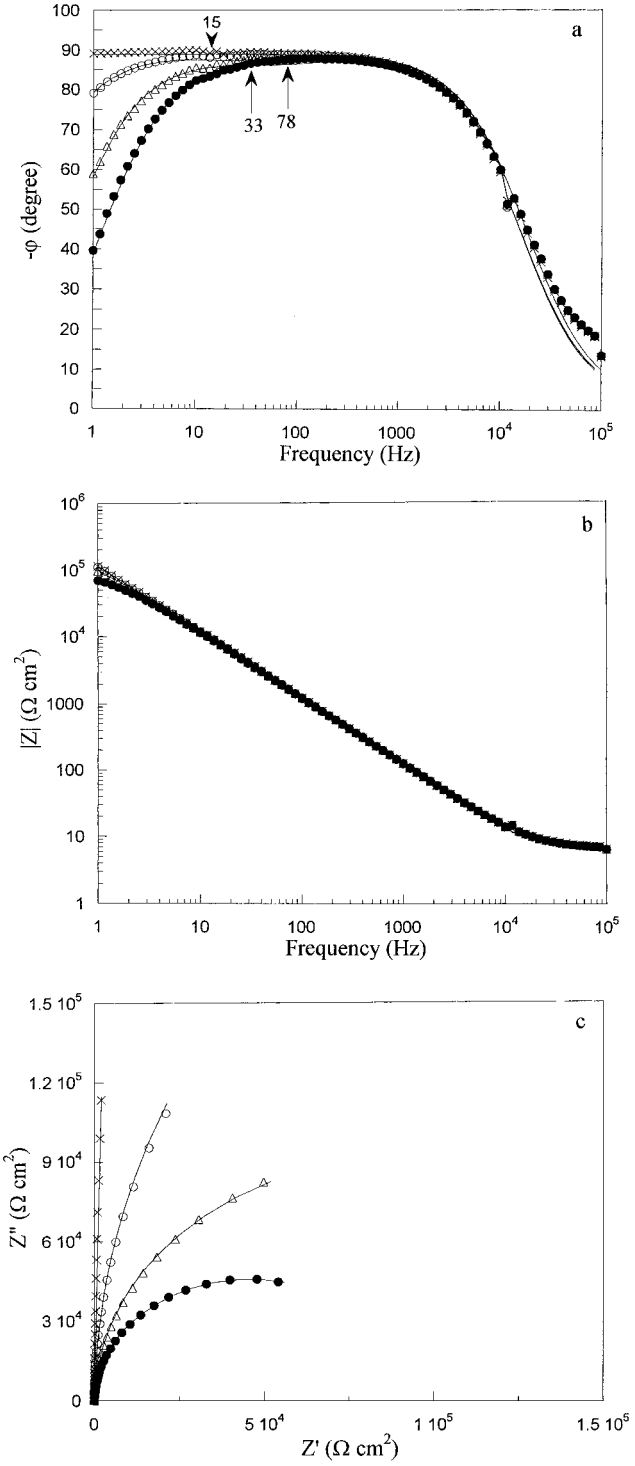

Figure 3. (a) Bode phase plot, (b) Bode plot, and (c) Nyquist plot of a $CH_3(CH_2)_{11}S$/Au SAM from +0.4 V (vs Ag/AgCl) to −0.2 V (×) (equivalent circuit I), at −0.3 V (○), −0.4 V (△), and −0.5 V (●) (equivalent circuit II) in 50 mM K_2HPO_4, pH 7.0. Symbols are the experimental data, and solid lines result from CNLS fits according to the equivalent circuits. The numbers in (a) correspond to the relaxation frequency, ν_d, tabulated in Table 1.

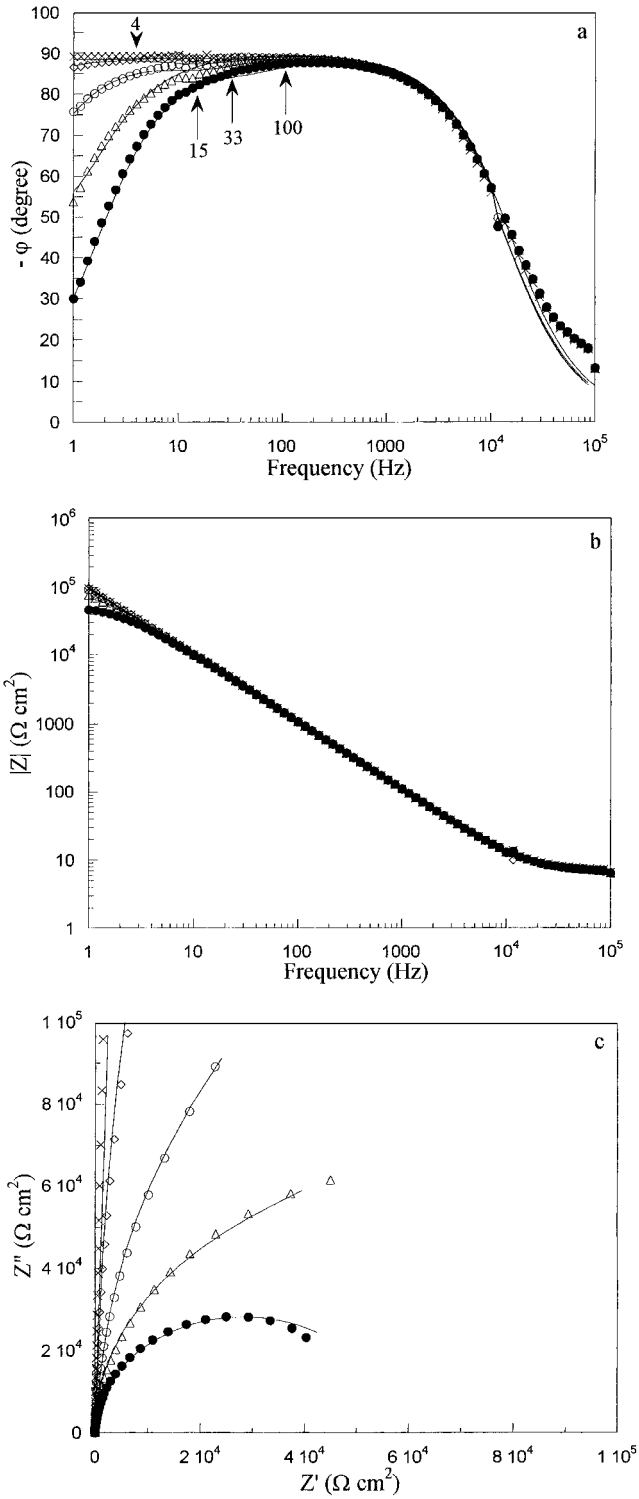

Figure 4. (a) Bode phase plot, (b) Bode plot, and (c) Nyquist plot of a $CH_3(CH_2)_7S$/Au SAM from +0.4 V (V vsAg/AgCl) to −0.1 V (×) (equivalent circuit I), at −0.2 V (◇), −0.3 V (○), −0.4 V (△), and −0.5 V (●) (equivalent circuit II) in 50 mM K_2HPO_4, pH 7.0. Symbols are the experimental data, and solid lines result from CNLS data fits according to equivalent circuits. The numbers in (a) correspond to the relaxation frequency, ν_d, tabulated in Table 1.

molecules and/or ions into the film. These experimental results do not, however, allow one to explicitly describe the sort of "defect" that has been formed. Extreme descriptions might include pores or holes. The field-induced perturbation of BLMs suggests that there are interesting parallels between SAMs and BLMs in that regard.[34,35] For BLMs, the sites of facilitated diffusion induced by large electric fields are believed to be microscopic regions having high-to-medium dielectric constants that permit ion transport across the bilayer.[63] In the BLM case, the critical electric field is $\sim 10^6$ V cm^{-1}.[64] The V_c data presented here (Table 1) translate into similar values. Accurate estimates would require knowledge of the exact thickness and potential of zero charge of the RS/Au SAMs. Nonetheless, it is apparent that the SAMs respond to an applied electric field in a fashion parallel to BLMs.

TABLE 1: Fitting Parameters Obtained of Defect-Free SAMs (Equivalent Circuit I, CPE and *n*) and Potential-Induced Defect SAMs (Equivalent Circuit II, C_m, R_m, C_d, R_d, and Relaxation Frequency ν_d)

equivalent circuit 2a			equivalent circuit 2b				
E, V	CPE, μF cm^{-2}	a	C_m, μF cm^{-2}	R_m, kΩ cm^2	C_d, nF	R_d, MΩ	ν_d, Hz
			$CH_3(CH_2)_7S$/Au SAM				
0.4	1.80 ± 0.06	0.986 ± 0.005					
0.3	1.70 ± 0.02	0.984 ± 0.001					
0.2	1.61 ± 0.02	0.989 ± 0.002					
0.1	1.50 ± 0.10	1.000 ± 0.009					
0	1.59 ± 0.02	0.989 ± 0.002					
−0.2			1.46 ± 0.01	92 ± 31	2.9 ± 0.5	97 ± 53	3.6 ± 1.9
−0.3			1.46 ± 0.02	48 ± 10	4.6 ± 0.5	16 ± 1.5	15 ± 1.5
−0.4			1.46 ± 0.01	48 ± 8	6.9 ± 1.0	5 ± 0.3	33 ± 4.8
−0.5			1.46 ± 0.02	15 ± 3	6.2 ± 1.2	2 ± 0.4	100 ± 20
			$CH_3(CH_2)_9S$/Au SAM				
0.4	1.67 ± 0.05	0.976 ± 0.004					
0.3	1.55 ± 0.02	0.975 ± 0.001					
0.2	1.41 ± 0.08	0.989 ± 0.008					
0.1	1.40 ± 0.02	0.985 ± 0.002					
0	1.28 ± 0.09	1.000 ± 0.010					
−0.1	1.28 ± 0.08	1.000 ± 0.009					
−0.2	1.36 ± 0.02	0.986 ± 0.002					
−0.3			1.20 ± 0.01	50 ± 12	2.8 ± 0.4	53 ± 13	6.6 ± 1.6
−0.4			1.20 ± 0.01	50 ± 12	4.1 ± 0.5	11 ± 0.8	20 ± 2.4
−0.5			1.24 ± 0.01	56 ± 4	6.2 ± 0.5	7 ± 0.2	25 ± 2.0
			$CH_3(CH_2)_{11}S$/Au SAM				
0.4	1.44 ± 0.01	0.987 ± 0.001					
0.3	1.42 ± 0.01	0.988 ± 0.001					
0.2	1.42 ± 0.01	0.987 ± 0.001					
0.1	1.43 ± 0.01	0.986 ± 0.001					
0	1.44 ± 0.01	0.986 ± 0.001					
−0.1	1.43 ± 0.01	0.986 ± 0.001					
−0.2	1.43 ± 0.01	0.986 ± 0.001					
−0.3			1.27 ± 0.01	54 ± 11	2.4 ± 0.23	28 ± 2.3	15 ± 1.4
−0.4			1.27 ± 0.01	36 ± 6.6	3.6 ± 0.42	7.3 ± 0.4	33 ± 3.9
−0.5			1.27 ± 0.01	14 ± 2.3	3.3 ± 0.28	3.9 ± 0.1	78 ± 6.6
			$CH_3(CH_2)_{15}S$/Au SAM				
0.4	1.07 ± 0.03	0.970 ± 0.004					
0.3	1.09 ± 0.01	0.988 ± 0.001					
0.2	1.08 ± 0.01	0.893 ± 0.002					
0.1	1.07 ± 0.01	0.981 ± 0.002					
0	1.01 ± 0.08	1.000 ± 0.010					
−0.1	1.03 ± 0.06	0.996 ± 0.008					
−0.2	1.05 ± 0.13	1.000 ± 0.012					
−0.3	1.11 ± 0.01	0.983 ± 0.002					
−0.4			0.95 ± 0.01	79 ± 12	5.2 ± 0.8	9 ± 0.7	20 ± 3.1
−0.5			0.96 ± 0.01	52 ± 5	12 ± 2.2	3 ± 0.2	25 ± 4.5

[a] ν_d = dielectric frequency = $(C_dR_d)^{-1}$. Values for C_d and R_d are not normalized for the electrode surface area.

It is important to emphasize that the critical potential, V_c, described here is clearly not due to the cathodic electrodesorption of the individual $CH_3(CH_2)_nS$ chains from the gold substrate. Table 2 summarizes the literature reductive electrodesorption potentials (E_p) of alkanethiols adsorbed onto both Au single crystals and polycrystalline Au. E_p is chain length dependent and ranges from −0.73 V ($n = 2$) to −1.35 V ($n = 17$). Clearly, the values of the electrodesorption potentials are considerably more cathodic than V_c values reported here. The variation in E_p[65] has been suggested to arise from (i) the decrease in solubility of the desorbed molecule as n increases,[38,41] (ii) a dependence of the potential gradient across the SAM on n,[37] and (iii) a chain length dependence of the SAM permeability toward the electrolyte.[43] This later possibility, which has not yet been thoroughly investigated, would suggest that the hydrocarbon chain length controls the ease with which ions can be partitioned into the SAM. From that perspective, the critical potential (V_c) observed by ac impedance spectroscopy can be viewed as a precursor to the electrodesorption process observed in the −1.1 to −1.4 V region.

2. Time Scale of Processes in SAMs. The time scale of chemical and electrochemical processes is a key factor in the characterization of SAMs. The subcircuit (C_d in parallel to R_d) in equivalent circuit II accounts for the SAM modification induced by the dc applied voltage at $V_{appl} \leq V_c$, while the main circuit accounts for the properties of the intact SAM. The product $(R_dC_d)^{-1}$ yields the dielectric relaxation frequency, ν_d. ν_d has been used in the experimental characterization of polymers and ion-selective membranes and describes the rate at which a film can be charged (and discharged) by ions originating from the electrolyte. ν_d here is found to be strongly potential dependent and is (modestly) thickness dependent (Table 1). At −0.5 V (i.e., at $V_{appl} < V_c$), where defects are created in $CH_3(CH_2)_nS$/Au ($n = 7-15$) SAMs, ν_d varies from 4 to 100 Hz. These values are similar to those previously reported (1−10 Hz) for 4′-hydroxy-4-mercaptobiphenyl and ω-hydroxydecanethiol SAMs.[66]

The value of the relaxation frequency, ν_d, calculated using equivalent circuit II can also be estimated from the Bode phase plots (φ vs f). The onset of the decrease of φ, from ca. 88 at f

TABLE 2: Literature Cathodic Electrodesorption Potentials (E_p) of $CH_3(CH_2)_nS$/Au SAMs Obtained from Cyclic Voltammetry Studies in Alkaline Solution

chain length, *n* $CH_3(CH_2)_nS$/Au	E_p V vs Ag/AgCl	experimental conditions	ref
2	−0.73	0.5 M KOH, Au(111)	*a*
3	−0.80	0.1 M $KClO_4$/KOH, pH 10.5	*b*
	−0.89	0.5 M KOH, polycrystalline Au	*c*
5	−1.05	0.5 M KOH, polycrystalline Au	*d*
7	−0.96	0.5 M KOH, polycrystalline Au	*c*
8	−1.00	0.1 M $KClO_4$/KOH, pH 10.5	*b*
	−0.96	0.1 M KOH, Au(111)	*e*
	−1.00	0.1 M KOH, Au(111)	*f*
10	−1.07	0.5 M KOH, Au(111)	*a*
13	−1.10	0.10 M KOH, Au(111)	*g*
15	−1.11	0.1 M $KClO_4$/KOH, pH 10.5	*b*
	−1.06	0.5 M KOH, quasi-Au(111)	*h*
17	−1.35	0.5 M KOH, polycrystalline Au	*d*

[a] Imabayashi, S.-I.; Iida, M.; Hobara, D.; Feng, Z. Q.; Niki, K.; Kakiuchi, T. *J. Electroanal. Chem.* **1997**, *428*, 33−38. [b] Yang, D.-F.; Wilde, C. P.; Morin, M. *Langmuir* **1997**, *13*, 243−249. [c] Walczak, M. M.; Alves, C. A.; Lamp, B. D.; Porter, M. D. *J. Electroanal. Chem.* **1995**, *396*, 103−114. [d] Widrig, C. A.; Chung, C.; Porter, M. D. *J. Electroanal. Chem.* **1991**, *310*, 335−359. [e] Yang, D.-F.; Al-Maznai, H.; Morin, M. *J. Phys. Chem. B* **1997**, *101*, 1158−1166. [f] Yang, D.-F.; Wilde, C. P.; Morin, M. *Langmuir* **1996**, *12*, 6570−6577. [g] Badia, A.; Arnold, S.; Scheumann, V.; Zizlsperger, M.; Mack, J.; Jung, G.; Knoll, W. *Sens. Actuators B* **1999**, *54*, 145−165. [h] Nishizawa, M.; Sunagawa, T.; Yoneyama, H. *J. Electroanal. Chem.* **1997**, *436*, 213-218.

< ∼100 Hz (shown by arrows in Figures 1a−4a), to smaller values is at about the same relaxation frequency values as the ν_d calculated from CNLS data fits (Table 1). No specific features can, however, be observed at ν_d in the other types of impedance plots ($|Z|$ vs f or Z'' vs Z'). The behavior of φ over a wide frequency domain thus provides a unique and direct tool for the characterization of SAMs and shows that important information can be obtained without resorting to an equivalent circuit analysis. The relaxation frequency ν_d is only obtained when $V_{appl} \leq V_c$ and corresponds to the SAM having a resistive component associated with the formation of defects.

It is important to note that the time during which a SAM is poised at $V_{appl} \leq V_c$ could be important. Many electrochemical studies of SAMs use relatively fast potential cycling and potential limits that greatly exceed the V_c values determined here. We do not presently know what the relationship between the extent of damage and the residence time in the $V_{appl} \leq V_c$ region is. This issue is currently under investigation.

3. Reversibility of the Potential-Induced Defects. As described, V_{appl} alters the SAM/electrolyte interface in a chain length dependent fashion. The changes observed in φ, R_m, C_d, R_d, and ν_d at $V_{appl} \leq V_c$ are consistent with the size and/or the number of the local defects becoming increasingly pronounced as V_{appl} increases in magnitude.

The reversibility of the potential-induced perturbation was studied by returning each SAM ($n = 7-15$) to 0 V immediately after the polarization at −0.5 V. Plots of φ vs f obtained at −0.5 V (Figure 5, open symbols) and subsequently at 0 V (filled symbols) suggest that the dc potential induces changes that are partially reversible since φ_{1Hz} returns to a large extent (> 81°) to its maximum value (≥88°). This is a good indication that $CH_3(CH_2)_nS$/Au SAMs are substantially but not completely restored to their initial electrical function. The potential excursion to $V_{appl} < V_c$ causes the SAM capacitance, C_m, to increase 8-fold (from 1.46 μF cm^{-2} at −0.5 V to 11.7 μF cm^{-2} at 0 V) for $n = 7$ and 7-fold (from 1.24 μF cm^{-2} at −0.5 V to 9.3 μF cm^{-2} at 0 V) for $n = 9$. The change in C_m is negligible, however, for $n = 11$ (from 1.27 to 1.28 μF cm^{-2}) and for $n = 15$ (from 0.96 μF cm^{-2} to 0.99 μF cm^{-2}). Ion insertion is clearly more pronounced for $n \leq 9$.

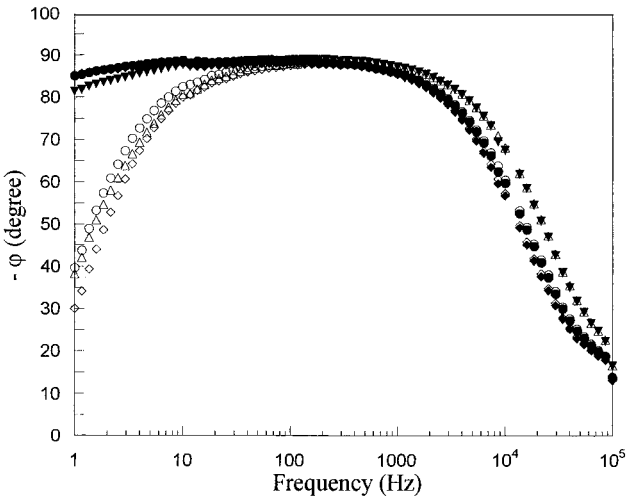

Figure 5. Investigation of the reversibility of potential-induced defects of $CH_3(CH_2)_nS$/Au SAMs for $n = 7$ (◇), $n = 11$ (○), and $n = 15$ (▽) at −0.5 V (open symbols) followed by dc polarization at 0 V (filled symbols). For defect-free SAMs, the phase angle at $f <$ ∼30 Hz remains ≥88°.

4. Conclusions and Overview. Detailed ac impedance spectroscopy measurements reveal unique electrochemical properties of *n*-alkanethiols SAMs formed on polycrystalline gold surfaces. Of particular note here is that a hitherto unreported change in these SAMs is detectable using ac EIS. This change is induced by the applied dc potential. At potentials more anodic than a critical potential (V_c), SAMs ($n = 7-15$) are ionic insulators. A SAM transformation is observed at applied potentials more cathodic than V_c and is associated with the formation of potential-induced defects. These defects render the SAM permeable to ions and/or water at $V_{appl} < V_c$. For *n*-alkanethiol SAMs ($n = 7-15$), V_c is chain length dependent and occurs between −0.15 and −0.35 V vs Ag/AgCl, potentials distant from reductive thiol electrodesorption. The chain length dependence of V_c is consistent with the change being related to the electrical breakdown experienced by thin organic films and lipid membranes. An awareness of the sensitivity of a SAM to potential-induced structural changes is particularly important given that many electrochemistry/redox probe studies (unknowingly) traverse V_c during measurement.

A detailed analysis of an appropriate equivalent circuit at various applied dc potentials leads to a relationship between each electrical component and the microstructural/molecular changes at the interface and/or inside the SAM. At $V_{appl} \leq V_c$, Bode phase plots (φ *vs* f) access the relaxation frequency ν_d of ion diffusion-related phenomena in $CH_3(CH_2)_nS$/Au SAMs, where ν_d is typically between 4 and 100 Hz. The potential-induced defects are not completely reversible over the time scale of these experiments.

Acknowledgment. The authors gratefully thank Antonella Badia for the synthesis of hexadecanethiol. This research project was financially supported by NSERC, FCAR, and a Grant-in-Aid of research from Sigma Xi to E.B.

References and Notes

(1) Evans, S. D.; Ulman, A. *Chem. Phys. Lett.* **1990**, *170*, 462−466.
(2) Cohen, R.; Bastide, S.; Cahen, D.; Libman, J.; Shanzer, A.; Rosenwaks, Y. *Opt. Mater.* **1998**, *9*, 394−400.

(3) Campbell, I. H.; Rubin, S.; Zawodzinski, T. A.; Kress, J. D.; Martin, R. L.; Smith, D. L.; Barashkov, N. N.; Ferraris, J. P. *Phys. Rev. B* **1996**, *54*, R14321−R14324.
(4) Janata, J.; Josowicz, M. *Anal. Chem.* **1997**, *69*, 293A-296A.
(5) Novotny, V. J.; Karis, T. E. *Appl. Phys. Lett.* **1997**, *71*, 52−54.
(6) Zenou, N.; Zelichenok, A.; Yitzchaik, S.; Cohen, R.; Cahen, D. *ACS Symp. Ser.* **1998**, *695*, 57−66.
(7) Zehner, R. W.; Parsons, B. F.; Hsung, R. P.; Sita, L. R. *Langmuir* **1999**, *15*, 1121−1127.
(8) Collet, J.; Vuillaume, D. *Appl. Phys. Lett.* **1998**, *73*, 2681−2683.
(9) Vuillaume, D.; Fontaine, P.; Collet, J.; Deresmes, D.; Garet, M.; Rondelez, F. *Microelectron. Eng.* **1993**, *22*, 101−104.
(10) Stora, T.; Lakey, J. H.; Vogel, H. *Angew. Chem., Int. Ed. Engl.* **1999**, *38*, 389−392.
(11) Terrettaz, S.; Stora, T.; Duschl, C.; Vogel, H. *Langmuir* **1993**, *9*, 1361−1369.
(12) Stelzle, M.; Weissmuller, G.; Sackmann, E. *J. Phys. Chem.* **1993**, *97*, 2974−2981.
(13) Raguse, B.; Braach-Maksvytis, V.; Cornell, B. A.; King, L. G.; Osman, P. D. J.; Pace, R. J.; Wieczorek, L. *Langmuir* **1998**, *14*, 648−659.
(14) Gafni, Y.; Weizman, H.; Libman, J.; Shanzer, A.; Rubinstein, I. *Chem. Eur. J.* **1996**, *2*, 759−766.
(15) Finklea, H. O. *Electrochemistry of Organized Monolayers of Thiols and Related Molecules on Electrodes*; Marcel Dekker: New York, 1996; Vol. 19, Chapter 2.
(16) Finklea, H. O.; Snider, D. A.; Fedyk, J.; Sabatini, E.; Gafni, Y.; Rubinstein, I. *Langmuir* **1993**, *9*, 3660−3667.
(17) Amatore, C.; Savéant, J. M.; Tessier, D. *J. Electroanal. Chem.* **1983**, *147*, 39−51.
(18) Nahir, T. M.; Bowden, E. F. *Electrochim. Acta* **1994**, *39*, 2347−2352.
(19) Sluyters-Rehbach, M.; Sluyters, J. H. *Sine wave methods in the study of electrode process*; Marcel Dekker:Amsterdam, 1970; Vol. 4.
(20) Badia, A.; Back, R.; Lennox, R. B. *Angew. Chem., Int. Ed. Engl.* **1994**, *33*, 2333−2334.
(21) Alonso-Romanowski, S.; Gassa, L. M.; Vilche, J. R. *Electrochim. Acta* **1995**, *40*, 1561−1567.
(22) Steinem, C.; Janshoff, A.; Ulrich, W.-P.; Sieber, M.; Galla, H.-J. *Biochim. Biophys. Acta* **1996**, *1279*, 169−180.
(23) Gassa, L. M.; Vallejo, A. E.; Alonso-Romanowski, S.; Vilche, J. R. *Bioelectrochem. Bioenerg.* **1997**, *42*, 187−192.
(24) Steinem, S.; Janshoff, A.; Wegener, J.; Ulrich, W.-P.; Willenbrink, W.; Sieber, M.; Galla, H.-J. *Biosens. Bioelectron.* **1997**, *12*, 787−808.
(25) Gritsch, S.; Nollert, P.; Jahnig, F.; Sackmann, E. *Langmuir* **1998**, *14*, 3118−3125.
(26) Steinem, C.; Janshoff, A.; von dem Bruch, K.; Reihs, K.; Goossens, J.; Galla, H.-J. *Bioelectrochem. Bioenerg.* **1998**, *45*, 17−26.
(27) de Levie, R.; Seidah, N. G.; Larkin, D. *J. Electroanal. Chem.* **1974**, *49*, 153−159.
(28) de Levie, R. *J. Electroanal. Chem.* **1975**, *58*, 203-216.
(29) de Levie, R. *Adv. Chem. Phys.* **1978**, *37*, 99−137.
(30) Ding, L.; Li, J.; Wang, E.; Dong, S. *Thin Solid Films* **1997**, *293*, 153−158.
(31) Steinem, C.; Janshoff, A.; Galla, H.-J.; Sieber, M. *Bioelectrochem. Bioenerg.* **1997**, *42*, 213−220.
(32) Schulze, K.-D. *Chem. Phys.* **1998**, *238*, 495−505.
(33) Vallejo, A. E.; Gervasi, C. A.; Gassa, L. M. *Bioelectrochem. Bioenerg.* **1998**, *47*, 343−348.
(34) Tsong, T. Y. *Biophys. J.* **1991**, *60*, 297−306.
(35) Weaver, J. C.; Chizmadzhev, Y. A. *Bioelectrochem. Bioenerg.* **1996**, *41*, 135−160.
(36) Haag, R.; Rampi, M. A.; Holmlin, R. E.; Whitesides, G. M. *J. Am. Chem. Soc.* **1999**, *121*, 7895−7906.
(37) Walczak, M. M.; Alves, C. A.; Lamp, B. D.; Porter, M. D. *J. Electroanal. Chem.* **1995**, *396*, 103−114.
(38) Yang, D.-F.; Wilde, C. P.; Morin, M. *Langmuir* **1997**, *13*, 243−249.
(39) Yang, D.-F.; Wilde, C. P.; Morin, M. *Langmuir* **1996**, *12*, 6570−6577.
(40) Imabayashi, S.-I.; Iida, M.; Hobara, D.; Feng, Z. Q.; Niki, K.; Kakiuchi, T. *J. Electroanal. Chem.* **1997**, *428*, 33−38.
(41) Badia, A.; Arnold, S.; Scheumann, V.; Zizlsperger, M.; Mack, J.; Jung, G.; Knoll, W. *Sens. Actuators B* **1999**, *54*, 145−165.
(42) Nishizawa, M.; Sunagawa, T.; Yoneyama, H. *J. Electroanal. Chem.* **1997**, *436*, 213-218.
(43) Yang, D.-F.; Wilde, C. P.; Morin, M. *Langmuir* **1997**, *13*, 243−249.
(44) Lang, H.; Duschl, C.; Vogel, H. *Langmuir* **1994**, *10*, 197−210.
(45) Zha, F. F.; Coster, H. G. L.; Fane, A. G. *J. Membr. Sci.* **1994**, *93*, 255−271.
(46) Macdonald, J. R. In *Complex Nonlinear Least Squares Immittance Fitting Program, LEVM 7.0*; Macdonald, J. R., Ed.: Department of Physics and Astronomy, University of North Carolina: Chapel Hill, NC., 1990.
(47) Macdonald, J. R. *Impedance Spectroscopy*; Wiley: New York, 1987.
(48) Furniss, B. S.; Hannaford, A. J.; Rogers, V.; Smith, P. W. G.; Tatchell, A. R. *Vogel's Textbook of Practical Organic Chemistry*, 4th ed.; Longman: New York, 1978.
(49) McAdams, E. T.; Jossinet, J. *Physiol. Meas.* **1995**, *16*, A1−A13.
(50) Boubour, E.; Lennox, R. B. *Langmuir* **2000**, *16*, 4222−4228.
(51) Helmholtz, H. *Ann. Phys.* **1879**, *7*, 337−382.
(52) Halliday, D.; Resnick, R. *Physics*; Wiley: New York, 1978.
(53) Hagenstrom, H.; Schneeweiss, M. A.; Kolb, D. M. *Langmuir* **1999**, *15*, 2435−2443.
(54) Mansfeld, F. *Electrochim. Acta* **1993**, *38*, 1891−1897.
(55) Mitton, D. B.; Latanasion, R. M.; Bellucci, F. *J. Electrochem. Soc.* **1996**, *143*, 3307−3316.
(56) Jennings, G. K.; Munro, J. C.; Yong, T.-H.; Laibinis, P. E. *Langmuir* **1998**, *14*, 6130−6139.
(57) Sondag-Huethorst, J. A. M.; Fokkink, L. G. L. *Langmuir* **1992**, *8*, 2560−2566.
(58) Sondag-Huethorst, J. A. M.; Fokkink, L. G. L. *J. Electroanal. Chem.* **1994**, *367*, 49−57.
(59) Sondag-Huethorst, J. A. M.; Fokkink, L. G. L. *Langmuir* **1995**, *11*, 2237−2241.
(60) Porter, M. D.; Bright, T. B.; Allara, D. L.; Chidsey, C. E. D. *J. Am. Chem. Soc.* **1987**, *109*, 3559−3568.
(61) Becka, A. M.; Miller, C. J. *J. Phys. Chem.* **1993**, *97*, 6233−6239.
(62) Swietlow, A.; Skoog, M.; Johansson, G. *Electroanalysis* **1992**, *4*, 921−928.
(63) Miyamoto, V. K.; Thompson, T. E. *J. Colloid Interface Sci.* **1967**, *25*, 16−25.
(64) Tien, H. T. *Bilayer Lipid Membranes (BLM): Theory and Practice*; Marcel Dekker: New York, 1974.
(65) Widrig, C. A.; Chung, C.; Porter, M. D. *J. Electroanal. Chem.* **1991**, *310*, 335−359.
(66) Janek, R. P.; Fawcett, W. R.; Ulman, A. *J. Phys. Chem. B* **1997**, *101*, 8550−8558.